Engineering Geology 312 (2023) 106928

Contents lists available at ScienceDirect

Engineering Geology

journal homepage: www.elsevier.com/locate/enggeo

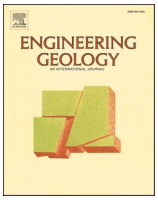

Centrifuge modelling of an expansive clay profile using artificial fissuring to accelerate swell

T.A.V. Gaspar [a,*], S.W. Jacobsz [a], G. Smit [a], A. Gens [b], D.G. Toll [c], A.S. Osman [c]

[a] Department of Civil Engineering, University of Pretoria, Pretoria, South Africa
[b] Department of Civil and Environmental Engineering, Universitat Politecnica de Catalunya - CIMNE, Barcelona, Spain
[c] Department of Engineering, Durham University, United Kingdom

ARTICLE INFO

Keywords:
Expansive soils
Centrifuge modelling
Partial saturation
Suction

ABSTRACT

This paper presents the results of a centrifuge study in which swell of an expansive clay profile was induced in the centrifuge. A factor which has previously hindered such research is the time required to induce significant swell in-flight, within a reasonable time frame. In this study the use of an artificially fissured fabric together with geotextile layers allowed for a significant magnitude of swell to be achieved within a matter of hours. Measurements of matric suction and water content throughout testing highlight the potential difficulties associated with such measurements in a fissured profile. The suction in clay along the interfaces of fissures can be significantly reduced almost instantaneously with the ingress of water. In contrast, elements closer to the centre of intact masses may take significantly longer to respond, illustrating the role of the dual processes (and hence dual scaling laws) of moisture ingress along fissures, followed by diffusion associated with swelling of the clay. A comparison of the magnitude of swell induced in this centrifuge model with that of conventional oedometer swell tests indicated gross overpredictions from the oedometer testing. In this comparison, the severe limitation of oedometer tests reducing a sample to a point of zero suction is emphasised. Finally, it is illustrated how an understanding of the rate of swell throughout an expansive profile can provide insights into the validity of the predictions from oedometer swell tests.

1. Introduction

The widespread occurrence of swelling or active clays has plagued engineers across the world for decades. While the expansive properties of such clays can be useful in certain instances (e.g. barriers for long-term storage of radioactive waste (Bosch et al., 2021)), when encountered in their natural state in situ, their behaviour is often problematic. Typically characterised as high plasticity clays which undergo significant seasonal volumetric changes, this type of problem soil presents many difficulties to foundation and structural design. Expansive clay deposits can also extend to great depths, further complicating the implementation of even deep foundations. In Kimberley, South Africa, expansive clay profiles have been found to extend to a depth of up to 30 m (Byrne et al., 2019). Other instances of deep expansive soils have also been reported in Sudan, where it is not uncommon to have expansive clay profiles extending to greater than 10 m in depth (Elsharief, 2012). Furthermore, this soil type also poses challenges from a testing perspective. Considering that such soils often occur in a highly fissured state in-situ (Chandler and Apted, 1988; Han et al., 2022; Ng et al., 2003; Jiang et al., 2018), samples tend to break apart either during the sampling process on site, or during extrusion in the laboratory. This creates a natural bias towards element testing of stronger, less fissured samples (Thorne, 1984). The presence of a highly fissured macrofabric also leads to incorrect measurements of hydraulic conductivity and processes associated with the movement of water (Toll et al., 2018; Novak et al., 2000; Van Genuchten et al., 1999). An example of such a discrepancy is provided by Clayton et al. (1995) who reported gross underestimations of the coefficient of consolidation from laboratory testing of fissured clays, in comparison to full-scale field measurements.

It is therefore particularly advantageous to perform full-scale testing for problems involving expansive clays (Blight, 1984a, 1984b; Brackley and Sanders, 1992; Meintjes, 1991; Meintjes and Pellissier, 1994). Despite the many advantages of full-scale testing, such studies are both costly and time-consuming due to the low hydraulic conductivity that is characteristic of these clays. A particularly extreme example of such a study was reported by Williams (1991) where heave continued for a period of 10 years.

* Corresponding author.
E-mail address: tiago.gaspar@durham.ac.uk (T.A.V. Gaspar).

https://doi.org/10.1016/j.enggeo.2022.106928
Received 4 November 2021; Received in revised form 8 November 2022; Accepted 14 November 2022
Available online 17 November 2022
0013-7952/© 2022 The Authors. Published by Elsevier B.V. This is an open access article under the CC BY license (http://creativecommons.org/licenses/by/4.0/).

List of notations

e	void ratio
N	centrifuge model scaling factor
$\bar{p}$	net-mean stress
s	suction
S_r	degree of saturation

The geotechnical centrifuge is a useful tool that can provide a compromise between the well-controlled boundary conditions possible with element testing, and the advantage of testing a larger sample. Testing scaled models at higher centrifugal accelerations also allow for consolidation and swell processes to be significantly accelerated. Despite its increased use to model a variety of geotechnical problems, it appears that centrifuge modelling has not been extensively exploited in the research of expansive clays. This is highlighted by the fact that only three publications on the subject have been presented at the last three International Conferences on Physical Modelling in Geotechnics (Laporte et al., 2018; Plaisted and Zornberg, 2010; Gu et al., 2010). Arguably the main challenge with the physical modelling of expansive clays is the time required for water to infiltrate a soil profile such that significant swelling can occur. This challenge has been mitigated by the use of auger holes in centrifuge models, to mimic the presence of fissures (Gu et al., 2010). Other studies have resorted to wetting the profile at 1 *g* over prolonged periods, prior to centrifuge testing (Chen et al., 2017). Chen et al. (2017) reported implementing this approach whereby the centrifuge model was wetted at 1 *g* for approximately 6–8 h. The results of this methodology indicated that increases in water content were mostly confined to the upper portion of the profile. It was also revealed that after several wetting and drying cycles, increases in water content were only seen to extend to the depth of shallow desiccation cracks. Another common theme from the above tests is that water has always been introduced from the surface. It could be argued that this is the most common method by which the water content of a soil is increased. However, there are a number of case studies which report increases in water content from beneath a structure, after evaporation has been cut off (Blight, 1984a, 1984b; Meintjes, 1991; Williams, 1991). This is an issue which can be exacerbated by the removal of vegetation (Blight, 1984a, 1984b). Such scenarios are arguably more hazardous to the overlying structures since moisture changes are allowed to occur over a substantially longer time frame in comparison to a precipitation event.

This study therefore utilises a novel sample preparation procedure to achieve swell in the centrifuge within a short time frame. The results of the centrifuge modelling conducted are then compared to oedometer swell tests and discussed within the framework on unsaturated soil mechanics principles. Such results and discussions allowed for the hydromechanical behaviour throughout the swell process to be investigated.

2. Basic soil characterisation

The clay tested in this study is a clay of extremely high plasticity (BSI 1377–2, 1990), sampled from the Limpopo province in South Africa. The material was sampled from the upper 1.5 m of the profile and can be described as a stiff, fissured and slickensided black clay containing fine nodular calcrete (Day, 2020). Preliminary tests conducted on intact samples revealed average values of gravimetric water content, void ratio, and degree of saturation of 33%, 0.977, and 90% respectively.

Basic classification tests were performed to establish the soil's particle size distribution (by method of sieving (ASTM, 2017a) and hydrometer (ASTM, 2017b)), Atterberg limits (ASTM, 2017c) and specific gravity (ASTM, 2014a). These results, as well as the unified soil classification (ASTM, 2017d) and British classification (BS 1377–2, 1990) are presented in Fig. 1 and Table 1. X-ray diffraction testing to determine the mineralogical composition of the clay was performed on the same site by a previous researcher, the results of which are shown in Table 2.

To provide additional characterisation of the clay studied, a one-dimensional consolidation test was performed on a reconstituted sample prepared at a water content of 1.1 times the soil's liquid limit. Loads were incrementally increased to a maximum stress of 1 MPa, with an average of 48 h allowed between load increments. After the 48 h there were no measurable changes in sample height, and so the consolidation stage was deemed complete. This test allowed for the intrinsic clay properties to be determined in accordance with the framework outlined by Burland (1990). The results of this consolidation test are presented in Fig. 2. Since infiltration was a key aspect of this study, the relationship between the saturated hydraulic conductivity calculated using consolidation theory ($k_{sat} = c_v . m_v . \gamma_w$) and void ratio is also illustrated in Fig. 2. The intrinsic compression index ($C_c^* = e_{100}^* - e_{1000}^*$) and void ratio at the clay's liquid limit (e_L) are 0.54 and 2.44 respectively.

3. Characterisation of swell properties

The mechanical properties of both compacted and undisturbed samples of the clay considered in this study was presented by Gaspar et al. (2022). The following section presents a summary of the oedometer tests conducted to quantify the swell properties of the tested clay. A series of oedometer tests were conducted to measure swell characteristics of the clay used for centrifuge modelling. For the swell tests, data is presented for both compacted and undisturbed specimens (prepared from block samples). In doing so, the extent to which the laboratory prepared specimens replicated the undisturbed swell behaviour could be assessed.

Recognising the difficulties associated with preserving the fissured macrofabric of expansive clays during the sampling process, the preparation procedure implemented was aimed towards introducing a certain degree of fissuring for samples prepared in the laboratory. The introduction of fissuring was particularly necessary for this study as it facilitates the ingress of water. The fissured fabric type was achieved by breaking down intact lumps of clay with a cheese grater at their in-situ water content (approximately 31%) and statically compacting the broken-down clay to a targeted dry density of 1350 kg/m^3. These initial conditions were selected as they are representative of the measured in-situ properties of the clay after the dry season. The rationale for targeting properties related to this season is that they present the most critical case if swell properties are to be measured (i.e. assessing the soil in its driest practical state allows for the largest estimates of swell magnitude and swell pressure to be obtained).

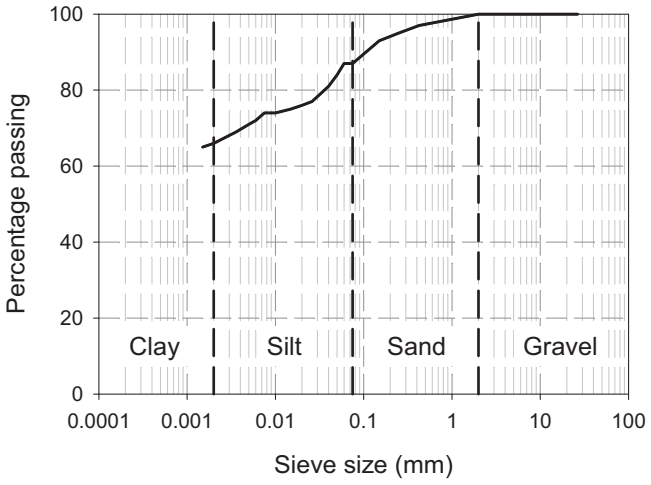

Fig. 1. Particle size distribution.

Table 1
Soil classification data.

Liquid limit (%)	92
Plasticity index	55
Linear shrinkage (%)	25.5
Activity	0.8
Specific gravity	2.65
Unified soil classification	CH
BS classification	CE

Table 2
Mineralogical composition based on X-ray diffraction (after Moses, 2008).

Mineral	Composition (%)
Smectite	58
Palygorskite	19
Calcite	5
Plagioclase	5
Quartz	4
Enstatite	4
Kaolinite	3
Diopside	2

This preparation procedure differs slightly from more conventional approaches whereby air-dried soil is mixed with a predetermined quantity of water, allowed to equilibrate, and compacted to a target dry density (Monroy et al., 2015; Manca et al., 2016). The drawback of this more conventional approach, however, is that it results in a fabric with macropores which are relatively isolated. Vanapalli et al. (1999) highlighted that for clayey soils compacted wet of optimum, pore spaces are in an "occluded" state. Such a fabric type was shown to increase the magnitude of suction required for desaturation (particularly at higher water contents), which would in turn, reduce hydraulic conductivity. Considering that the in-situ water content of the clay considered was approximately 90% (as noted previously) such an approach to sample preparation was deemed inadequate to produce the fissured macrofabric more typical of expansive clays.

To investigate the swell properties of the compacted and undisturbed specimens, a series of *wetting after loading* (ASTM D4546–14, 2014b) sometimes referred to as *swell under load* tests, were conducted at various applied stresses. Such tests involve placing an unsaturated sample into the oedometer, applying a predetermined stress (referred to as the soaking stress) and then flooding the housing with distilled water. As the sample is inundated, volumetric changes are monitored until such point that these changes become negligible. Once volumetric changes cease, the sample is considered as having reached a state of zero suction (Schreiner, 1988) and the final volumetric strain is noted for that stress level. The reason for using this testing procedure over other alternatives (e.g. loading after wetting tests (ASTM D4546–14, 2014b) or constant volume swell tests ((Brackley, 1973; Sridharan et al., 1986; Rao, 2006)) is that it represents a stress path most typically followed in typical construction sequences (Schreiner and Burland, 1991). Furthermore, it is the stress path that was followed in the centrifuge model presented. Table 3 presents the initial sample properties for the oedometer swell tests. Fig. 3 illustrates the results of wetting after loading tests for both the compacted and undisturbed specimens conducted at several values of applied vertical stress. Linear regression curves have also been superimposed onto the dataset for both the compacted and undisturbed samples.

From Fig. 3 it can be seen that the measured swell properties of the compacted and undisturbed specimens are similar. The similarities between the two regression curves were assessed by calculating the differences between the curves at each data point between 12.5 and 500 kPa and assessing the hypothesis of whether the average of the differences was equal to zero. A Student's t test indicated that an average difference of zero can be accepted with a confidence level of 80%. Such

Table 3
Initial sample properties for oedometer swell tests.

Description	Soaking stress (kPa)	Void ratio, e	Gravimetric water content, w (%)	Degree of saturation, S_r (%)	Dry density (kg/m^3)
Compacted	12.5	0.969	33.6	91.9	1346
Compacted	25	0.971	33.6	91.6	1344
Compacted	50	0.908	30.3	88.5	1389
Compacted	100	0.938	32.2	90.9	1367
Compacted	200	0.973	34.6	94.4	1343
Compacted	300	1.037	34.6	88.6	1301
Compacted	400	1.027	34.6	89.4	1307
Undisturbed	12.5	0.939	31.5	89.0	1367
Undisturbed	25	0.888	30.3	90.5	1403
Undisturbed	50	0.817	29.5	95.6	1459
Undisturbed	100	0.889	30.2	90.2	1403
Undisturbed	200	0.901	29.9	87.8	1394
Undisturbed	300	0.992	30.3	81.0	1331
Undisturbed	400	1.020	32.0	83.2	1312
Undisturbed	500	1.068	30.8	76.3	1281

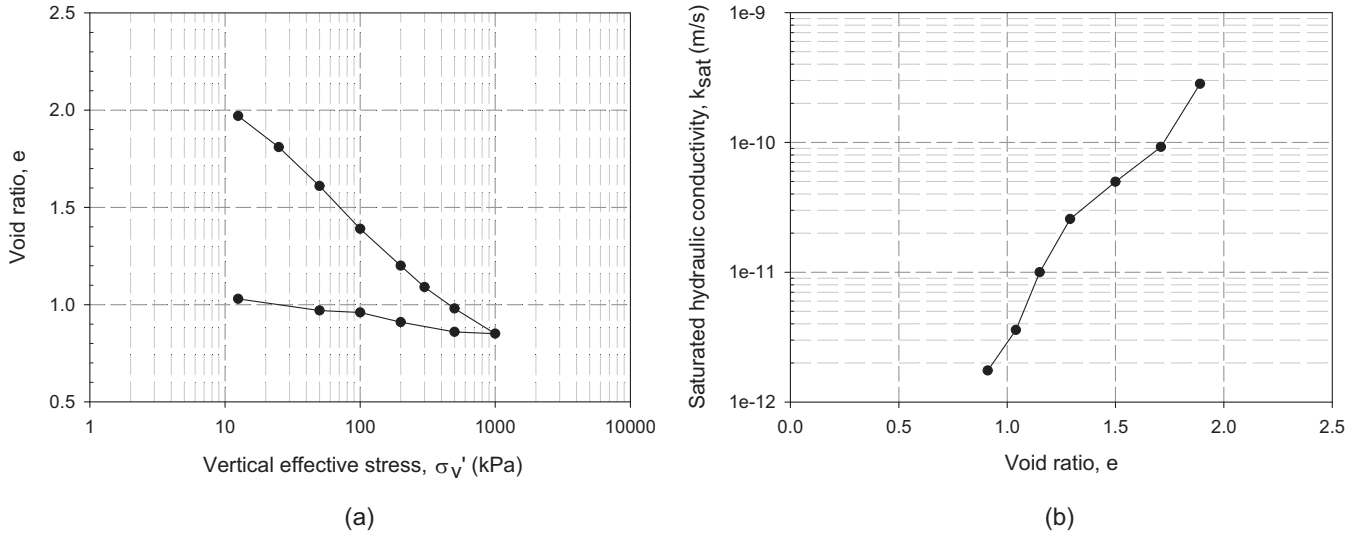

Fig. 2. One-dimensional consolidation test results illustrating the relationship between a) σ_v' and e, and b) k_{sat} and e.

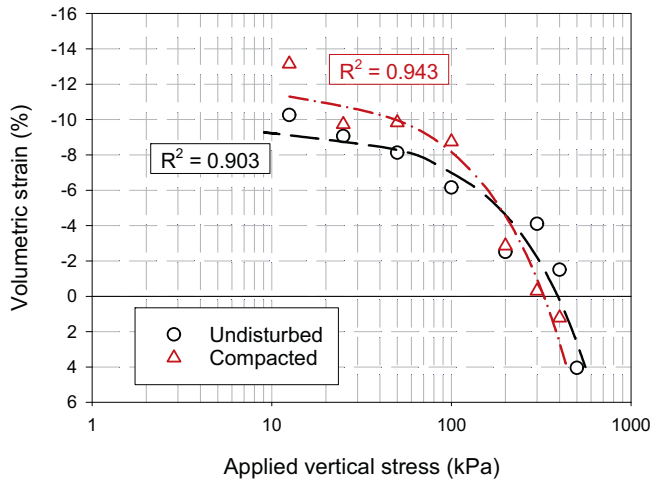

Fig. 3. Soaking under load curves for compacted and undisturbed samples.

results illustrate that the sample preparation procedure implemented was able to retain key characteristics of the undisturbed material. In light of this finding, the same approach was implemented in the preparation of the centrifuge model presented in the following section.

4. Model description

The centrifuge model presented in this study was conducted on the geotechnical centrifuge at the University of Pretoria (Jacobsz et al., 2014). All references to length and time in this section are presented in terms of model scale. Full-scale (prototype) dimensions can be obtained by multiplying model dimensions by the model scaling factor ($N = 30$) whereas the scaling laws relating to time and flow processes are discussed in the following section. The model layout (illustrated in Fig. 4) consisted of 5 statically compacted clay slabs (50 mm thick) separated by layers of needle-punched non-woven geotextile. Such geotextiles are commonly used in the construction industry for drainage/filtration systems. Their inclusion in this centrifuge model is therefore to facilitate the rapid ingress of water, rather than to provide any stiffness to the soil profile. The geotextiles were sized such that they could move freely in the vertical direction as swell occurred. Preparation of the clay slabs was conducted using the procedure described in the previous section. Initial properties of each slab are provided in Table 4. From this table it can be seen that the initial gravimetric water content of the clay slabs was an average of 3.5% less than that of the statically compacted samples prepared for oedometer testing. This can be attributed to the longer time required to prepare the centrifuge model, during which some moisture was lost. The lower water content is, however, consistent for all clay layers in the model. In Fig. 5, a photograph of the surface of a clay layer is presented. In this figure, the individual clay gratings and resulting "fissuring" can be seen.

The five clay slabs were laterally restrained in position by two perforated steel plates, covered with the same geotextile used to separate the clay layers. The two spaces on either side of the model were used as water wells to facilitate the ingress of water. Upon reaching the desired centrifugal acceleration of 30 *g*, water was introduced into the strongbox from the bottom. Water was continuously added over a period of 30 min, until the water level was approximately 20 mm above the surface of the top slab. This water level was maintained for the duration of testing (approximately 4.5 days in model time). Once the flooding process was complete, every clay layer had access to water on all four boundaries (top, bottom and sides). The front and back of the model were confined between the strongbox's glass window and an aluminium partition plate.

Table 4
Initial properties of clay layers.

Distance from bottom of model to layer surface	Layer number	Gravimetric water content, w (%)	Degree of saturation, S_r (%)	Void ratio, e	Dry density (kg/m^3)
52	1	30.1	75.0	1.06	1284
104	2	30.1	75.2	1.06	1286
156	3	29.7	72.5	1.09	1271
208	4	29.7	73.8	1.07	1282
260	5	29.8	72.6	1.09	1269

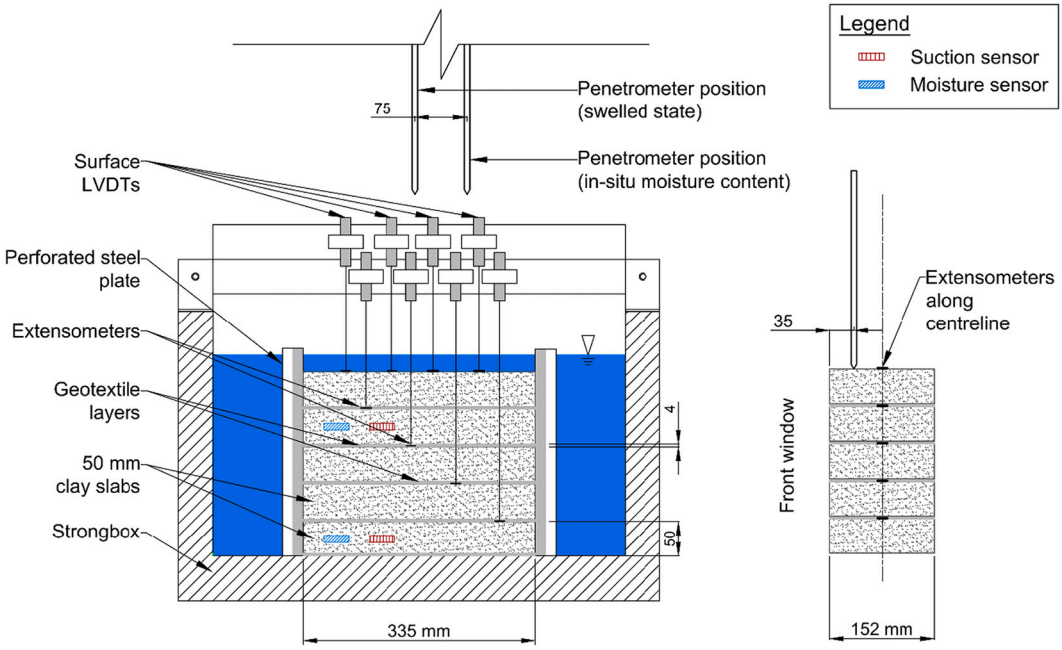

Fig. 4. Model layout.

Fig. 5. Photograph of the surface of a clay slab.

5. Model instrumentation

The instrumentation utilised in this centrifuge model included:

1. Linear variable differential transformers (LVDTs) and extensometers to measure the swell of each clay layer
2. Volumetric water content probes (Meter Group, 2017*a*)
3. Fixed matrix porous sensors (Meter Group, 2017*b*) for the measurement of soil suction.
4. A cone penetrometer to assess penetration resistance at the clay's initial and swelled state

As per the manufacturer's specifications at the date of purchase, details of the volumetric water content probes and suction sensors are presented in Table 5 and Table 6 respectively. To install the water content and suction sensors in the clay layers, static compaction of the slabs was performed with void formers in the desired positions of these sensors. Following compaction, these void formers were removed, leaving a space for the sensors to be installed. Clay gratings were then moulded around the sensors prior to installation, and any space behind them was backfilled with the same material. Due to the fact that the water content sensors exhibit an almost instantaneous response time, they could be installed immediately after the moulding of the clay. In contrast, the suction sensors have been shown to have a slow initial equilibration period (Tripathy et al., 2016). For this reason, suction sensors had to be prepared in advance.

Tripathy et al. (2016) showed that the measured value of suction is dependent on whether the suction sensor is installed in a wet or dry state. This tendency is related to the hysteretic properties of the sensor's ceramic discs. Furthermore, the initial state of the suction sensor was also shown to influence the time to achieve equilibrium. To assess these factors, and to determine the accuracy of the sensors, a preliminary test was conducted by installing two suction sensors in the same clay slab, one of which was installed 'wet' and the other, installed 'dry'. The clay slab was prepared to the same initial properties as those prepared for the centrifuge model with a gravimetric water content and void ratio of 31.5% and 1.07 respectively.

Table 5
Manufacturer specifications for volumetric water content probes (Meter Group, 2017a, 2017b).

	Apparent dielectric permittivity, K_a (unitless)
Range	1–80[†]
Resolution	Not specified
Accuracy	±1[*,‡]

[†] K_a = 1 when the sensor is held in air. K_a = 80 when the probe is immersed in water

[*] According to the manufacturer, this translates to an accuracy of ±0.03m^3/m^3 when using Topps' Equation for mineral soils (Topp, 1980).

[‡] Valid in the range K_a = 1–40 (0–0.4m^3/m^3). An accuracy of ± 15% of the measurement value applies outside this range

Table 6
Manufacturer specifications for fixed-matrix porous sensors (Meter Group, 2017a, 2017b; Tripathy et al., 2016).

	Matric suction (kPa)
Range	9–100,000
Resolution	0.1
Accuracy	±(10% of reading+2)[†]

[†] An accuracy is only reported for readings between 9 and 100 kPa

The wet sensor was allowed to soak in water until the measured suction was 9 kPa (reported to be the lower measurement limit of the sensor (Meter Group, 2017a, 2017b.; Tripathy et al., 2016)). Clay gratings were subsequently moulded around the sensor as prescribed in the manufacturer's user manual. For the dry sensor, the ceramic discs were removed and oven dried at 60 °C. After assembly, clay gratings were moulded around the ceramics. Whatman No. 42 filter papers were placed on the surface of the clay slab, and the entire setup was tightly wrapped with clingfilm and aluminium foil to avoid moisture loss (a technique suggested by Heymann and Clayton, 1999). On day 15, the clingfilm and foil were momentarily removed on one end of the slab, to place new filter papers for a second matric suction measurement. Fig. 6 illustrates the response of the two sensors over a period of 30 days. Discrete points indicate the suction measurements at day 7 and 20, and a

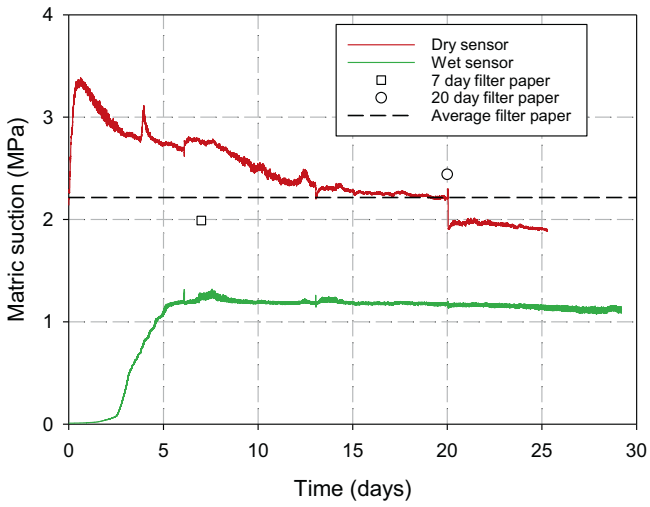

Fig. 6. Comparison of suction measurements made with fixed-matrix porous sensors and filter papers.

dotted line represents the average matric suction from the filter paper measurements.

Fig. 6 shows that, when filter papers were removed from the slab on day 20, the disturbance caused a sharp drop in measured suction of the 'dry' sensor. However, if the value before this drop is taken as being representative, it can be seen that the suction measured by this sensor closely matched the average suction measurement from the filter paper readings. Conversely, the sensor installed 'wet' equilibrated at a value of suction, approximately 1 MPa lower. Such a result is likely due to the hysteretic properties of the ceramic discs.

Based on the result in Fig. 6, it was decided that the sensors installed in the centrifuge model should be prepared from a 'dry' state. However, the equilibration period of approximately 20 days after installation in the clay, was deemed impractical for the purposes of this study. For this reason, it was decided that the initially dry sensors would be pre-equilibrated prior to installation in the centrifuge model. This was achieved by placing the sensors in a sealed chamber partially filled with distilled water and allowing the ceramics to slowly absorb water through vapour transfer. Suction measurements were then monitored until the sensors achieved the anticipated matric suction of the clay slabs (approximately 2 MPa). Clay gratings were then moulded around the sensor, and it was sealed for approximately 24 h until being installed in the centrifuge model. The resulting sensor equilibration is illustrated in Fig. 7. This approach allowed sensor equilibration to be carried out independently of the rest of the model setup.

In-flight cone penetration testing (CPTs) was used to assess the consistency of the preparation of each of the five layers. Furthermore, it provided an indication of the extent to which the clay softened during the swell process. To quantify the effects of swell-induced softening, two CPTs were performed. The first was performed at the clay's in-situ water content and matric suction. The 'post-swell' measurement was conducted at a magnitude of swell predicted by the Van der Merwe (1964) empirical prediction method for a clay of *very high potential expansiveness*. Being commonly used as an estimate of heave potential in Southern Africa, this value of swell was taken as representative of the swell magnitude which would be expected in situ. The Van der Merwe (1964) approach is based on observations of the movement of buildings founded in swelling clays. The procedure involves characterisation of the potential expansiveness of a clay based on its plasticity index and fraction of clay sized material. Based on this characterisation, the clay is assigned a magnitude of swell per unit layer thickness. An empirical factor is then introduced to account for the effect of overburden stress on swell magnitude. The swell magnitude at any position within the clay profile is then calculated using Eq. (1).

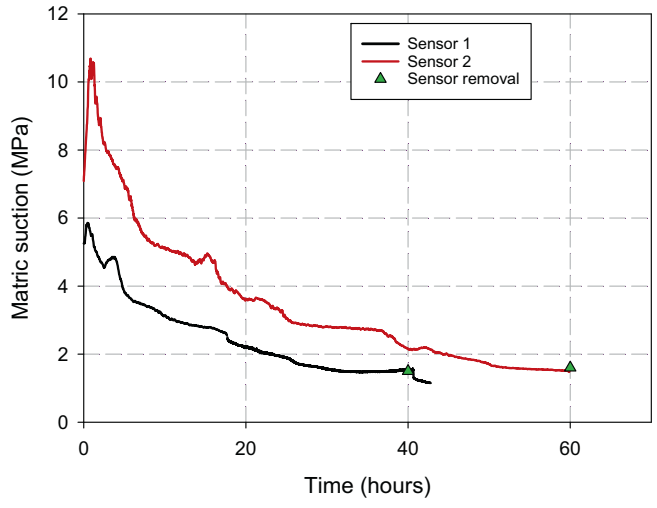

Fig. 7. Equilibration of suction sensors.

$$S = t \times h \times F \quad (1)$$

where:

S = swell (m)

t = thickness of expansive layer (m)

h = unit heave – dependent on characterisation of potential expansiveness (m/m)

F = empirical factor which reduces with depth along a clay profile

The penetrometer used was 8 mm in diameter with a 60° conical tip. The design used was based on that proposed by Carey et al. (2014). Details of the penetrometer used in this study are outlined by Gaspar (2020). It should be noted that the geotextiles separating the clay layers had 50 × 50 mm square cut-outs in the positions where CPTs were performed. The measured penetration resistances are provided in Fig. 8. Peak resistances correlate to the centre of the slabs with troughs representing the transitions between layers. The peaks being slightly out of phase can be attributed to differences in slab thicknesses after swell. It can be seen that the measured resistances prior to swell are remarkably consistent between layers, illustrating good repeatability in the slabs' preparation. Furthermore, penetration resistances measured at the soil's swelled state illustrate a similar reduction in strength for the bottom 4 layers, with greater softening occurring in the top slab.

6. Results and discussion

6.1. Swell magnitude and time for swell to occur

Fig. 9 illustrates the swell observed in each clay slab as well as the variation in surface swell across the width of the model. The swell percentages presented in Fig. 9 (a) were calculated as the ratio of the change in slab thickness, to initial slab thickness. For Fig. 9 (b) swell was calculated as the ratio of the change in thickness of the entire clay profile to its original thickness. In Fig. 9 (a) the slight slope change observed at around 45 h was due to an overnight drop in water level slightly below the surface of the clay profile. The water level was promptly topped up at

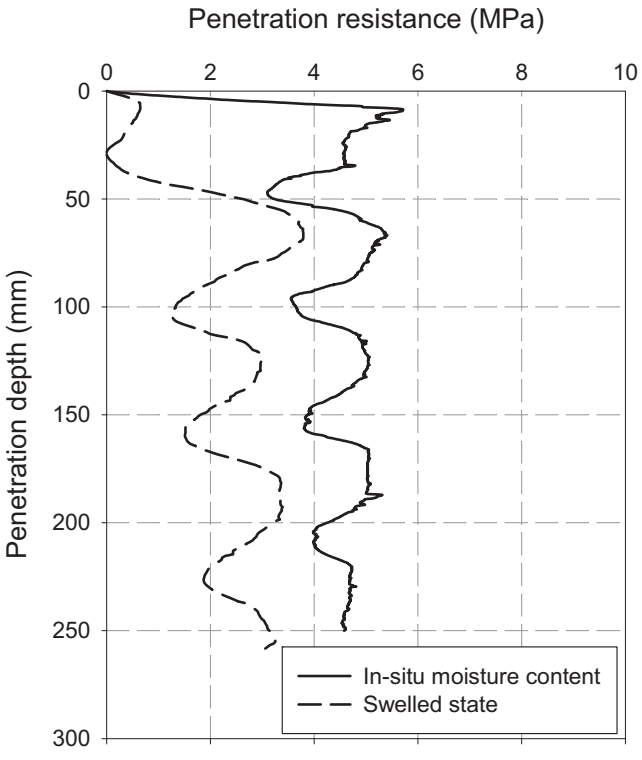

Fig. 8. Measured penetration resistances before and after swell.

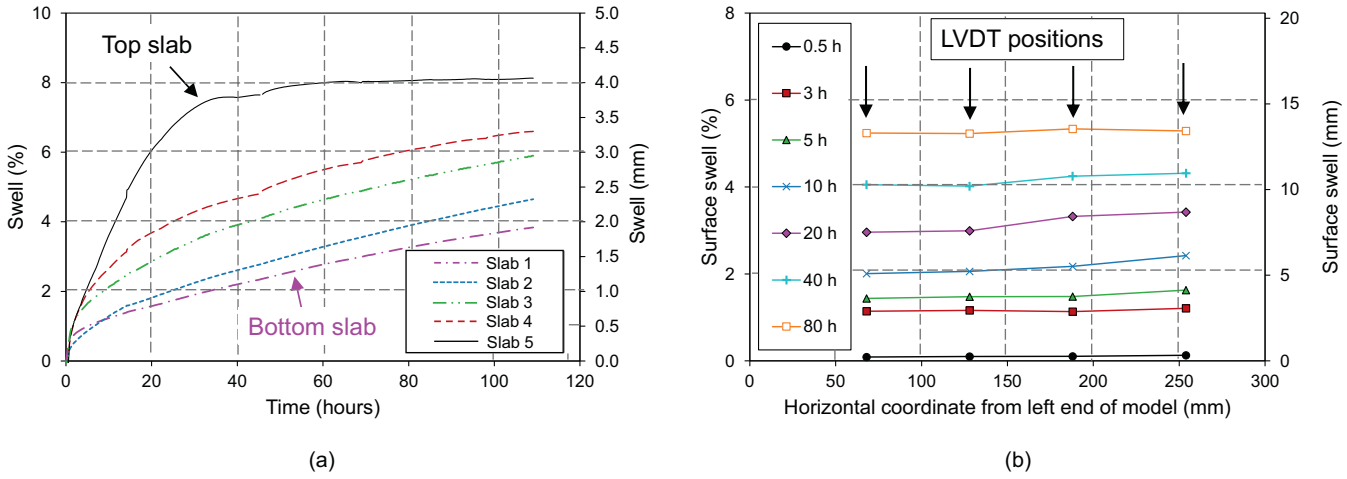

Fig. 9. Results illustrating: (a) swell versus time for each layer in the centrifuge model and (b) variation in surface swell along the width of the model.

this point and swell proceeded. In this figure, Slab 5 and Slab 1 correspond to the top and bottom slabs respectively. In Fig. 9 (b) the positions of the surface LVDTs are indicated at the top of the graph.

Fig. 9 (a) illustrates that, while the swell in the top slab began to illustrate negligible volume change at around 60 h, all slabs beneath it, subjected to higher overburden stresses, continued to show a slow increase in swell with time. Fig. 9 (b) illustrates that there was little variation in surface swell across the width of the profile, illustrating that boundary effects had an insignificant effect on swell.

While the results presented in Fig. 9 extend for a period of approximately 110 h, the targeted swell was achieved much sooner. Fig. 10 illustrates how the targeted swell of ≈ 7 mm at surface (predicted by Van der Merwe (1964) for a clay of *very high potential expansiveness*) was achieved at approximately 14 h.

The 14 h required to achieve the targeted swell equates to 525 days at prototype scale if model time (t) is scaled as $t^* = t \times N^2$, where t^* is the prototype time and N is the model scaling factor. In addition to its usage in scaling time for consolidation, Caicedo et al. (2006) illustrated that this scaling law is equally applicable to the process of swell from an unsaturated state. The implications of the significant time required to achieve the targeted swell are that, were a full-scale test to be conducted, the entire profile would need to be flooded for almost one and a half years before testing (e.g. soil-structure interactions) could be conducted at the targeted magnitude of swell. This result illustrates the benefit of the preparation procedure implemented in this study, i.e. development of closely fissured clay slabs separated by layers of geotextile.

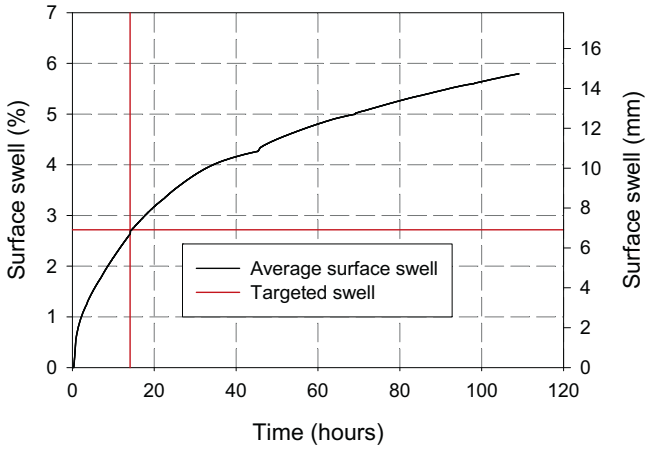

Fig. 10. Average measured surface swell.

6.2. *Water ingress, changes in suction and soil softening*

Another aspect of interest in this study is the reduction in matric suction as the model was flooded with water. Fig. 11 illustrates variations in matric suction and water content during inundation. From Fig. 11, it can be seen that matric suction in the bottom layer was reduced to approximately 9 kPa (the lower limit of the sensor) within two minutes. Layer 4 illustrates a more gradual reduction, occurring over 11 min. However, both measured changes occur significantly quicker than may be expected for a high plasticity clay with a saturated hydraulic conductivity, in the region of 10^{-9}–10^{-12} m/s (as shown in Fig. 2).

Considering the initial layer properties in Table 4, the accuracy of the initial volumetric water content (VWC) readings in Fig. 11 (b) can be assessed. For Layer 4, the initial VWC corresponds to a gravimetric water content (w) of 31%. This compares well with the value presented in Table 4 (w = 30%) obtained from measurements conducted on off-cuts from the various slabs. The VWC of Layer 1 however, corresponds to w = 41% which is 11% higher than that presented in Table 4. A possible explanation for this discrepancy could be attributed to local variations in dry density and water content in the vicinity of the VWC sensor. Nevertheless, the measured trend for this layer presented in Fig. 11 is still useful for the interpretation of the infiltration process. At the same instances that reductions in matric suction were observed in Fig. 11 (a), a corresponding increase in VWC is observed in both layers in Fig. 11 (b)

An explanation for the observed rapid changes in matric suction and VWC can be attributed to the presence of fissures acting as preferential flow paths. This is supported by the fact that the VWC increased to 100%, indicating a volume of solids equal to zero. Such a reading implies the presence of one or more fissures allowing a continuous film of water to span the individual prongs of the sensor.

This result raises the question of what value of suction may be used to adequately describe the behaviour of the mass clay profile (i.e. that measured along fissures, or that measured within the intact clay masses). To further explore this issue, consider the conceptualised wetting mechanisms presented in Fig. 12 which presents a mass-fissured clay profile at different stages of wetting. For simplicity, no volumetric changes have been presented.

In Fig. 12 (a), the profile consists of several intact clay masses, separated by air-filled fissures. As the soil is initially wetted, the surfaces of the various intact masses of clay may rapidly reduce to a point of zero suction. This is illustrated conceptually in Fig. 12 (b) where the outer regions of the clay masses correspond to the contour for a ‘wet state’. Quantitatively, this is represented by the result in Fig. 11. As the fissures close through swelling, the hydraulic conductivity of the entire soil mass

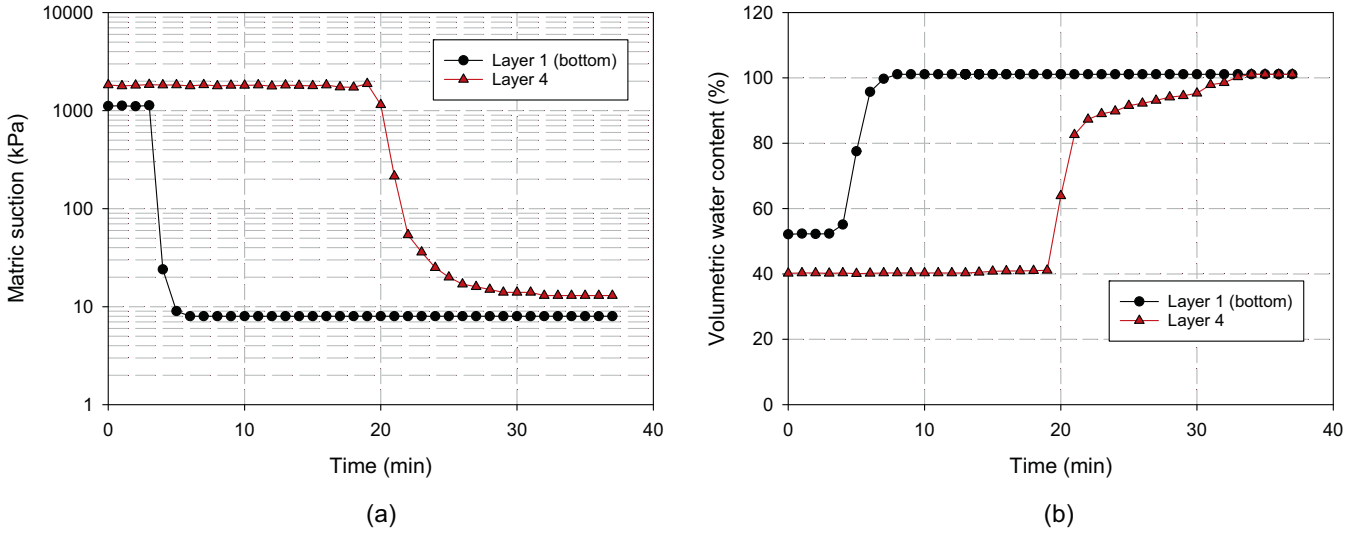

Fig. 11. In-flight measurements of a) matric suction and b) volumetric water content.

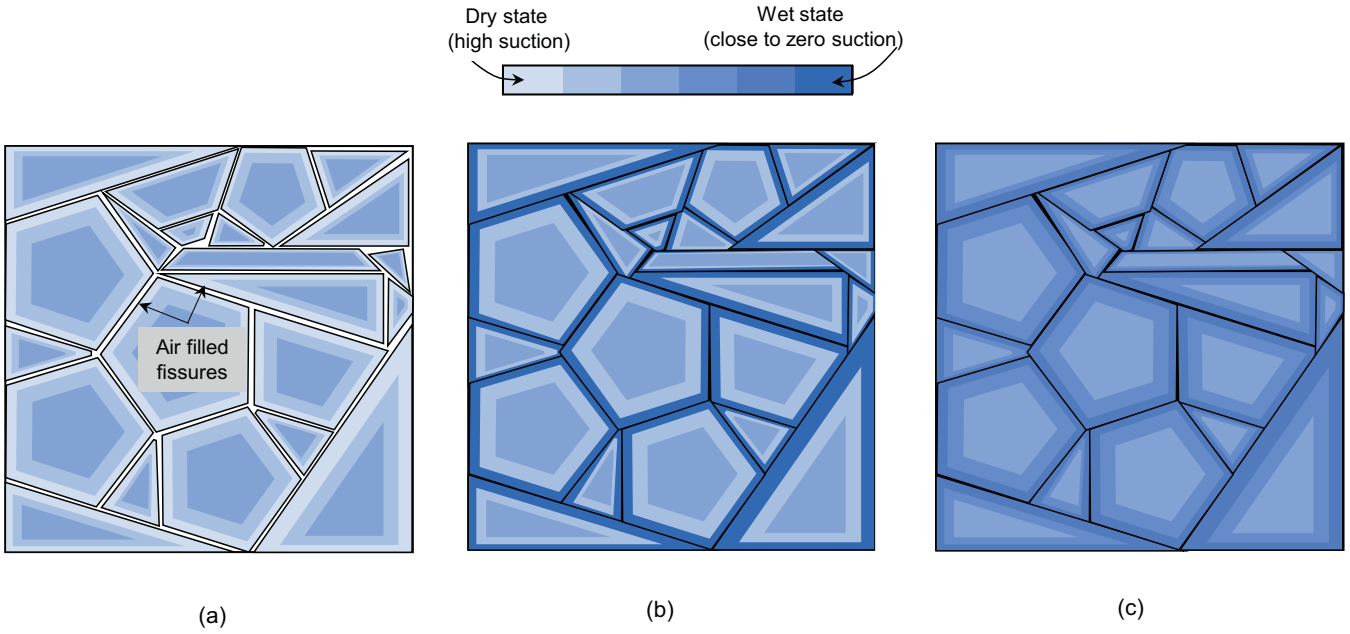

Fig. 12. Wetting process of an expansive fissured profile illustrating a) the in-situ ('dry') state of the clay mass, b) the clay mass after initial wetting and closure of fissures and c) some time after the closure of fissures where intact masses of clay tend towards an equilibrium value of suction.

will drop significantly (Fig. 12 (b)). Following the closure of the fissures and a drop in hydraulic conductivity, matric suction along the outer portions of the intact masses of clay will tend towards a point of equilibrium with the centres of these masses. This is illustrated in Fig. 12 (c) where the colour contours of the inner and outer portions of the clay masses tend towards a point of equilibrium.

By examining the infiltration process described in this section, it may be more accurate to state that two scaling laws are applicable when modelling a fissured clay. Initially, as water flows through the macro-fissures of the profile, the scaling law for seepage velocity is applicable, and so time should be scaled by a factor of N (where N is numerically equivalent to the model scaling factor). Once the fissures swell closed, the scaling law for a diffusion process proposed by Caicedo et al. (2006) becomes applicable and time should be scaled by N^2. Considering the swell percentages presented in Fig. 9 (a) and the surface heave in Fig. 10, it is observed that a small amount of swell occurred rapidly after the introduction of water. This rapid, but small increase in swell is believed to be associated with the filling of fissures, after which swell continued at a more gradual rate as suction equilibrium began to establish. Given the short duration of the infiltration phase and the fact that it scales linearly by the scale factor N, it appears that the duration of this phase can, for practical purposes, be ignored as it will be overshadowed by the much longer diffusion process which scales by N^2.

By examining the CPT results and the degree of swell in each clay layer, qualitative interpretations can be made as to the likely stress paths undergone by the soil during swell. If it is recognised that the behaviour of unsaturated soils can be described as both a function of suction and net stress (Bishop, 1959; Fredlund and Morgenstern, 1977; Alonso et al., 1990), it then becomes a point of interest as to what the relative contributions of these two mechanisms were. An estimate of net-mean stress

can be obtained by considering the total vertical stress at the start of testing, the magnitude of pressure required to prevent swell (i.e. swell pressure), and assuming $\sigma_2 = \sigma_3$ such that $\overline{p} = \left[\frac{1}{3}(\sigma_1 + 2\sigma_3) - u_a\right]$ (where the air pressure u_a is assumed to be atmospheric). From the initial sample data presented in Table 4, the average unit weight of the clay layers is 16.3 kN/m^3. The model presented in this study represents a 7.5 m profile at prototype scale. The vertical total stress at the bottom of the model can therefore be calculated to be ≈ 122 kPa. Throughout the swell process, if swell is perfectly restricted, it is plausible for the horizontal stress to be equivalent to the swelling pressure of the clay (mentioned previously to be ≈ 330 kPa). Using these values, the net-mean stress is calculated to be in the order of 191 kPa. The initial suction in the clay slabs was approximately 2 MPa. Despite the simplifying assumptions made in the estimation of net-mean stress, it can be seen that the initial suction of the clay in this model was an order of magnitude larger than the net-mean stress. It can therefore be assumed that suction (and the associated plastic deformations resulting from a reduction in suction) was the dominating factor contributing to shear strength, and that the net-mean stress component was, for all practical purposes, negligible. At the time that the second CPT was performed, the top slab had reached approximately 63% of its ultimate value of swell. After about 60 h, negligible volumetric changes were observed in this slab. Such a trend is typical of that observed for swell under load tests performed in the oedometer where the sample is typically referred to as reaching a point of "zero suction" (Schreiner, 1988).

Considering that the top slab had not quite reached steady state at the time the CPT was performed, it cannot be definitively stated that suction had reduced to zero. However, having achieved a higher degree of swell, it can be stated that the suction in this layer had been reduced by a greater amount. This interpretation is supported by the CPT data presented in Fig. 8. These results illustrate a 90% reduction in penetration resistance for the top slab. This is in contrast to the remaining four slabs in the centrifuge model which had markedly higher (but consistent) values of penetration resistance. While the top slab was free to swell in the vertical direction, the swell of subsequent slabs was restricted due to overburden stress. Fig. 9 also illustrates that even after the test was completed, the swell in these clay slabs had not approached a state of negligible volumetric change. The consistency in the penetration resistance of these slabs indicates that suction within the bottom four slabs was likely reduced by approximately the same amount.

6.3. Comparison of centrifuge swell with oedometer and empirical prediction methods

Where the consolidation settlement of a clay profile is crucial to geotechnical design, it is important to predict both the magnitude and rate of consolidation. The magnitude of consolidation settlement can be quantified reasonably accurately through the use of simple element-testing. If the rate of consolidation (coefficient of consolidation) is to be evaluated, much less accurate predictions are possible from element-testing since the soil fabric of laboratory samples are unrepresentative of field conditions (Clayton et al., 1995).

While these two aspects are relatively independent for consolidation problems, they are significantly more closely related for swell processes. Considering that consolidation is brought about by the increase and subsequent dissipation of excess pore water pressure (often due to the construction of a new structure/embankment), it is reasonable to state that the ultimate magnitude of consolidation settlement predicted from oedometer testing will be achieved *eventually*. Unless the additional stress of the structure/embankment is removed, the excess pore water pressure brought about by its construction must dissipate over time.

In contrast, the process of swell is brought about by a reduction in matric suction due to the ingress of water. Since changes in soil water content can arise due to short and isolated events (precipitation, leaking pipes, etc.), the ultimate magnitude of swell predicted from oedometer testing may never be achieved in practice if it does not occur within one wetting event. For this reason, to gain an understanding of the likely magnitude of swell that can be encountered, an understanding of the rate of swell within a profile is crucial. While more long-term wetting events are possible, e.g. due to preventing evaporation by construction of a foundation or removal of vegetation, such wetting mechanisms are not the focus of this discussion.

To explore this issue further, it is important to consider the volume of water the profile has access to, and the duration for which this volume of water is made available. For standard oedometer testing, an unlimited supply of water is made available to the sample for the period necessary to reduce the sample to a state of zero suction (i.e. where it begins to illustrate negligible volume changes with time). In practice, an expansive clay profile will typically be allowed access to a limited amount of water for a restricted time frame. For the centrifuge model presented in this study, the profile was allowed access to an unlimited volume of water for a restricted time. Fig. 13 illustrates comparisons of the results of the *wetting after loading* oedometer tests (for compacted samples) presented previously, the heave profile predicted by the Van der Merwe (1964) approach, as well as centrifuge swell measurements at various instances in time. The *wetting after loading* oedometer tests provided a relationship between percentage swell, and the magnitude of overburden stress on a sample. Using this relationship together with centrifuge model stresses and dimensions, the curve presented in Fig. 13 is obtained.

From Fig. 13 several observations can be made. Firstly, it can be seen that the measured swell in the centrifuge model at 14 h correlates closely with the Van der Merwe (1964) empirical heave prediction. Another point of interest is that both the empirical prediction and the centrifuge measurements at this instant follow a non-linear relationship of swell versus depth. This is in contrast to the predictions derived from oedometer (*wetting after loading*) tests which follow an approximately linear trend.

Recognising that oedometer swell tests are conducted until such point that volumetric strains show negligible changes with time (a state of zero suction), it can be stated that such predictions present an upper limit of the possible magnitude of swell. With this borne in mind, the rate of swell throughout the profile can be evaluated by investigating

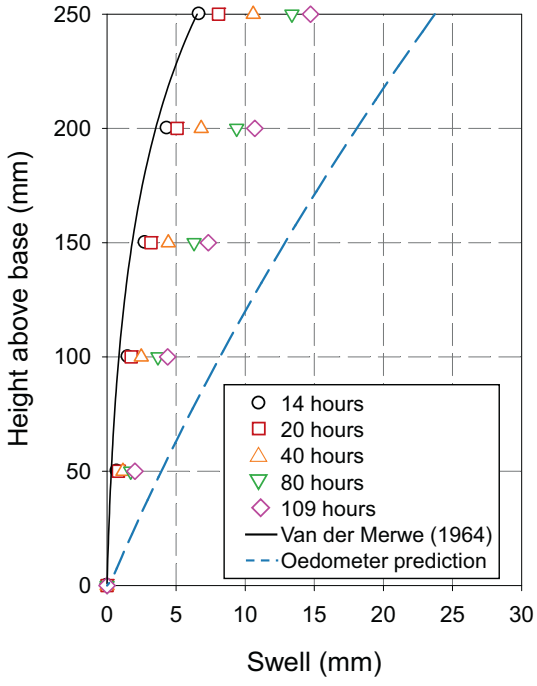

Fig. 13. Measured versus predicted swell.

how far along the swell process each layer is at a given instant in time (i.e. the degree of swell). Fig. 14 illustrates the ratio of centrifuge swell measured for each layer at a specific instant in time to the upper limit of swell (as determined from oedometer testing) for that particular layer. The vertical axis in this figure presents normalised depth throughout the profile where z is the depth below the clay surface and D is the total profile thickness.

From Fig. 14, it can be seen that the rate of swell is greater in the upper portions of the profile. If for example the isochrone representing the swell profile at 10 h is evaluated, the top layer had achieved approximately 32% of its upper limit of swell whereas the bottom layer had only progressed 16% through the swell process. Furthermore, the discrepancy in swell progression between the top and bottom layer increases with time until the upper layer approaches its maximum limit of swell. Once soil in the upper elements has achieved the maximum amount of swell, the bottom elements begin to 'catch up' and the difference between the top and bottom layers begins to decrease. This relationship is presented in Fig. 15. It is worth noting that, while Fig. 14 illustrates that the top layer of the model had only achieved 70% of its upper limit of swell, this 'upper limit' was determined from a separate set of oedometer samples. Based on results presented previously, it was stated that the top clay slab had in fact achieved a state of negligible volumetric change. It is therefore likely that the swell process in the top slab had completed at 80 h. Differences between the maximum amount of swell predicted by oedometer testing with that achieved in the centrifuge can be attributed to slight differences in initial sample properties.

These differences in the rate of swell can be attributed to differences in the evolution of hydraulic conductivity throughout the depth of the profile. Generally speaking, it can be stated that hydraulic conductivity is largely governed by soil fabric (Romero and Simms, 2008), void ratio, e, and degree of saturation, S_r.

The results presented in Fig. 2 (b) illustrate how the saturated hydraulic conductivity of the clay considered in this study can reduce by several orders of magnitude with a reduction in void ratio. Similarly, a reduction in suction (or increase in degree of saturation) will increase hydraulic conductivity by several orders of magnitude (Fredlund, 2018; Lu and Likos, 2004; Toll et al., 2018). Recognising that unsaturated hydraulic conductivity is generally represented as the product of saturated hydraulic conductivity (dependent on void ratio) and the relative permeability (dependent on changes in degree of saturation), changes in both these properties throughout a swell process will affect the rate of swell.

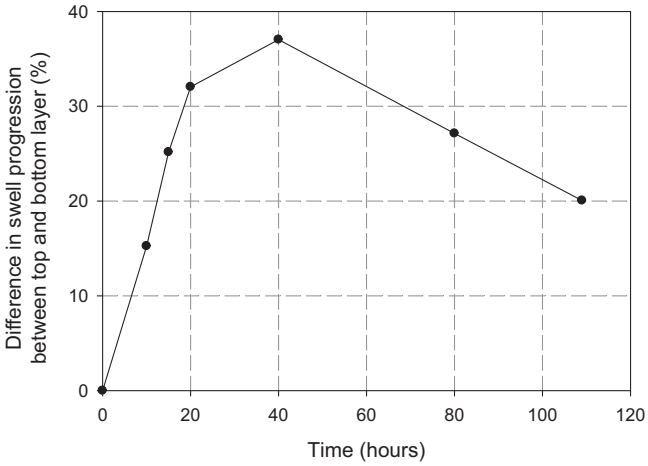

Fig. 15. Difference in swell between top and bottom layer.

However, since swell (or changes in void ratio) is suppressed deeper in the profile, the increase in hydraulic conductivity will occur at a slower rate for an element of soil at a significant depth, in comparison to one which is close to the surface. As a result, swell at the bottom of the profile will not only be restricted by overburden pressures, but significantly delayed owing to the lower hydraulic conductivity of these elements.

To illustrate this concept, consider and Fig. 16 a) and b) which describe the changes in hydraulic conductivity for an element of soil close to the surface, and deep in the profile respectively. In both figures, the three rectangles at the top illustrate the swell of a soil element. The elements are labelled t_1, t_2 and t_3. These labels represent the progression of time with t_1 corresponding to the instant at which the entire profile is given access to water, and t_2 and t_3 representing arbitrary points in time after swell had initiated. The instances t_1, t_2 and t_3 represent the same

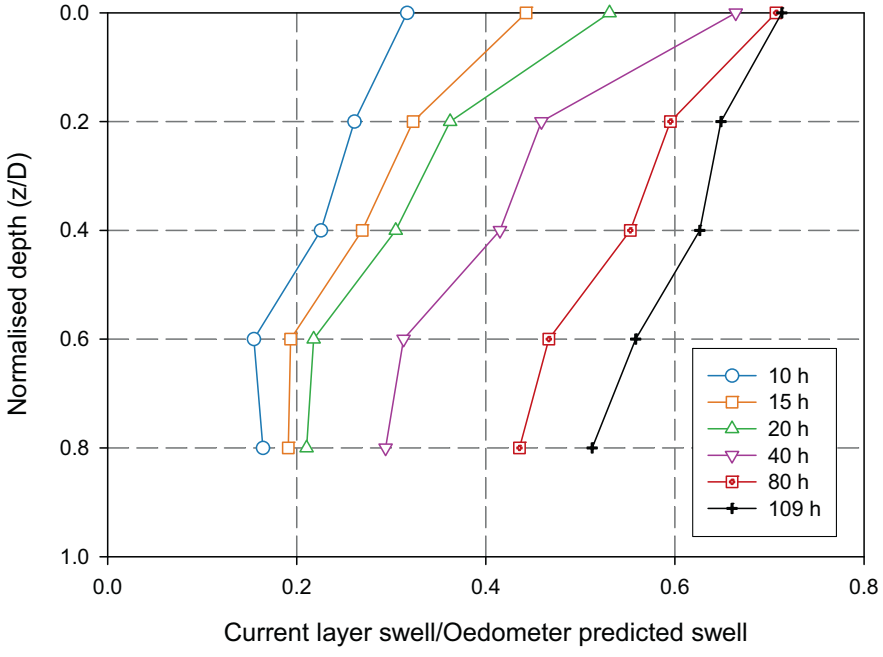

Fig. 14. Progression of swell with time.

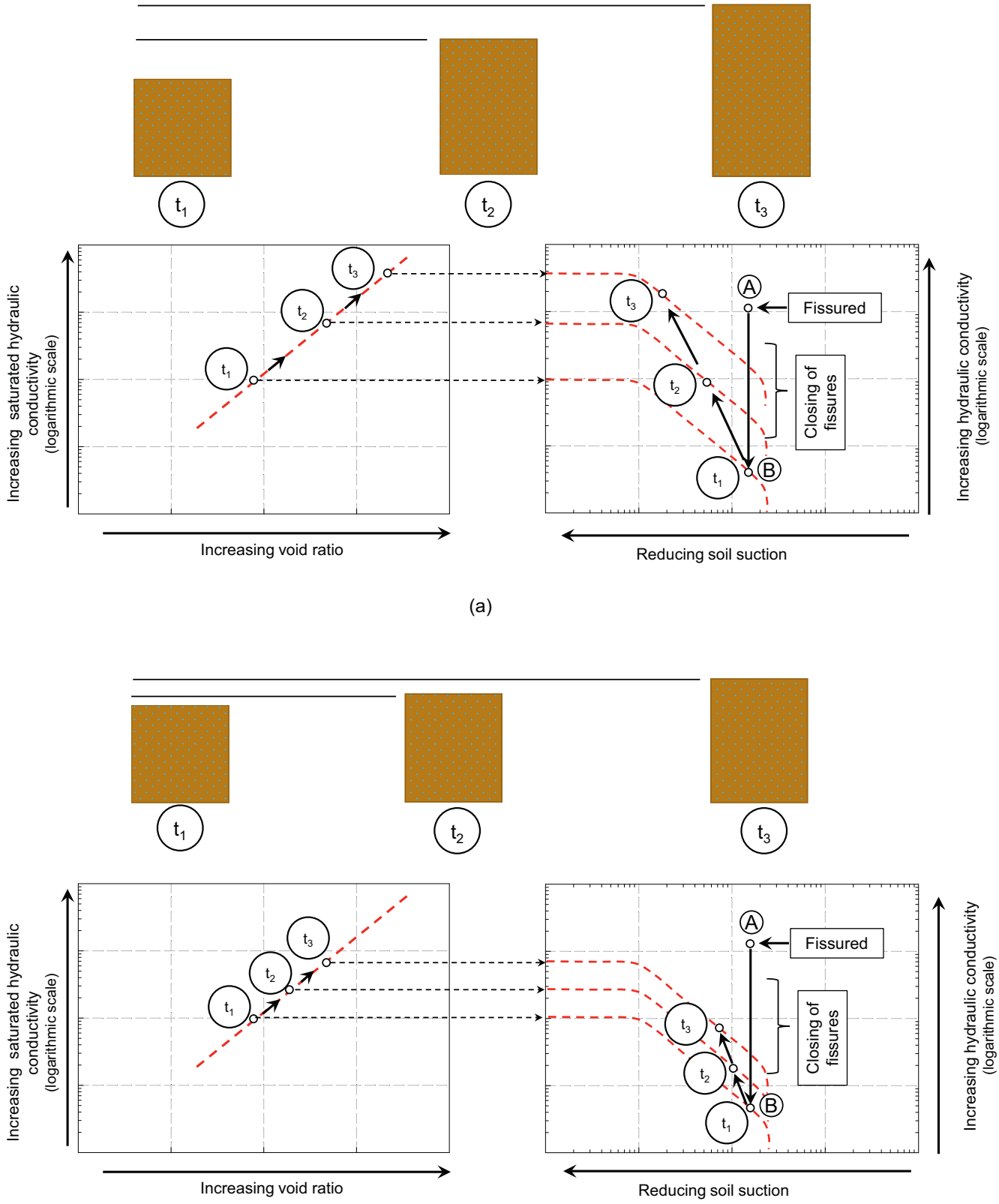

Fig. 16. Development of swell for an element of soil a) close to the surface of the profile and b) deep within the soil profile.

point in time for both figures. The two graphs presented in each figure describe the effect of a reduction in suction and an increase in void ratio on increasing the hydraulic conductivity. The suction-hydraulic conductivity relationship is typically represented as a hydraulic conductivity function (HCF). The HCFs presented, are those proposed by Fredlund (2018) which result from the mathematical integration of the soil water retention curve (SWRC). This trend is merely presented as a qualitative illustration of the interplay between suction and hydraulic

conductivity.

In Fig. 16 a) and b), an initial stage is illustrated whereby an increase in water content results in the closure of fissures (Path AB). This evolution in fabric occurs at the macro scale and is assumed to occur relatively quickly in the infiltration process. Considering the wetting process described in Fig. 12, it is also assumed that the suction in the soil mass remains relatively unchanged as fissures swell closed (i.e. the suction of the soil mass in Fig. 12 (b)).

In Fig. 16 a) and b), a general trend between saturated hydraulic conductivity (k_{sat}) and void ratio is illustrated as a dotted diagonal line. At the three time increments, values of k_{sat} govern the position of the hydraulic conductivity function (also illustrated as dotted lines), which translates upwards as the soil swells. The data points which represent different instances in time illustrate how, for an element of soil closer to the surface, greater increases in hydraulic conductivity are observed (as represented by the greater spacing between data points). The reason for this is that swell (i.e. increases in void ratio) are allowed to occur more freely at lower confining stresses. Conversely, for an element of soil deeper in the profile (where void ratio changes are largely restricted), data points are clustered closer together illustrating a smaller change in hydraulic conductivity over the same time frame.

In geotechnical practice, it is often assumed that only the upper portions of a clay profile are susceptible to volumetric changes since it is the upper regions which are most susceptible to seasonal fluctuations in moisture and are most free to swell (lower confinement). Such descriptions, however, provide only a partial explanation for such swelling behaviour. The implications of the above discussion together with the results presented in Fig. 9 a), are that the evolution of hydraulic conductivity throughout the depth of a profile plays a significant role in the ability of an expansive clay layer to achieve its upper limit of swell. By considering the evolution of hydraulic conductivity it can be stated that even if a wetting process were to occur at greater depths (e.g. due to a fluctuating water table), the long duration required for elements of soil in the lower portions of the profile to be reduced to a state of zero suction make it unlikely that their ultimate magnitude of swell will be achieved.

The conceptualisation of this infiltration process illustrates that, given an unlimited availability of water, an element of soil close to the surface will achieve the level of swell predicted by the *wetting after loading* tests first. In contrast, an element of soil deeper in the profile may take significantly longer (and is far less likely) to achieve the magnitude of swell predicted by oedometer testing. The description of hydraulic conductivity provided in this section provides an explanation as to why the upper clay layers in the centrifuge model achieved greater reductions in suction, despite water being introduced into the strongbox from the bottom. It also highlights why the Van der Merwe (1964) empirical prediction method predicts a non-linear heave profile, with greater swell occurring in the upper clay layers.

Recognising the mechanisms described in this section, observations of heave in the field should tend towards the predictions made by *wetting after loading* tests, given sufficient time and availability to water. Furthermore, predictions made from oedometer tests are far less likely to be achieved in practice for soil elements deeper in the profile. Conventional *wetting after loading* tests can therefore be regarded as indicator tests that provide the upper limit of swell which is theoretically possible (given certain initial soil conditions).

7. Conclusions

This study presents a centrifuge model demonstrating the swelling process in a highly expansive South African clay under greenfield conditions. Due to the low hydraulic conductivity associated with swelling clays, the long duration required to induce swell in the centrifuge has historically been a hindrance for such investigations. In this study, it was found that the combination of an artificially fissured sample fabric with the use of geotextiles allowed for a significant magnitude of swell (comparable to that predicted by a relevant empirical prediction method) to be achieved in-flight within approximately 14 h. Comparatively, the modelled process would take almost one and a half years of constant flooding at prototype (full) scale. Such a finding will allow for future studies to more easily consider aspects of soil-structure interaction throughout a typical swell process.

Measurement of a representative suction and water content has been found to be potentially problematic since a gradient of suction exists from the outer portions of an intact clay mass (along its fissures) to its centre. Along fissures, suction can be reduced almost instantaneously during a wetting process, whereas the suction at the centres of clay masses may take significantly longer to respond. Such a result is indicative of two processes (and hence scaling laws) of water seepage along fissures, followed by diffusion of water after fissures have swelled closed.

The non-linear relationship of swell magnitude with depth measured in the centrifuge was found to compare well with the empirical prediction method considered. Conversely, the results of oedometer swell tests presented by the authors were found to significantly overpredict swell in comparison to the centrifuge model.

The discrepancy between swell measured in the centrifuge and that observed in the field (Van der Merwe, 1964) with that predicted from oedometer testing is related to the evolution of hydraulic conductivity throughout an expansive clay profile.

After flooding the entire model, swell throughout the profile was simultaneously accompanied by an increase in void ratio and a reduction in suction, both of which are mechanisms that increase hydraulic conductivity. Since void ratio and water content vary by differing amounts throughout the profile during a swell process, so too will the hydraulic conductivity. As such, the increasingly more permeable upper portion of a clay profile tends towards the upper boundary of swell predicted by conventional oedometer tests, whereas elements of clay deeper in the profile will respond significantly slower. It is therefore far more likely that elements of clay closer to the soil surface will achieve their upper limit of swell. Recognising the differences in wetting processes between oedometer testing and in-situ conditions, it is emphasised that conventional oedometer swell tests are simply indicators of the upper limit of swell possible (given an initial void ratio and water content).

CRediT authorship contribution statement

T.A.V. Gaspar: Conceptualization, Methodology, Formal analysis, Investigation, Writing – original draft, Visualization. **S.W. Jacobsz:** Conceptualization, Supervision, Funding acquisition, Writing – review & editing, Project administration. **G. Smit:** Conceptualization, Methodology, Writing – review & editing. **A. Gens:** Conceptualization, Writing – review & editing. **D.G. Toll:** Conceptualization, Writing – review & editing. **A.S. Osman:** Conceptualization, Funding acquisition, Writing – review & editing, Project administration.

Declaration of Competing Interest

The authors declare that they have no known competing financial interests or personal relationships that could have appeared to influence the work reported in this paper.

Data availability

Data will be made available on request.

Acknowledgements

The authors gratefully acknowledge the financial support from the UK Engineering and Physical Sciences Research Council (EPSRC) under the Global Challenges Research Fund for the project “Developing performance-based design for foundation systems of WIND turbines in

AFRICA (WindAfrica)", Grant Ref: EP/P029434/1. The authors also thank Rick Vandoorne and Paul le Roux for reviewing this paper and providing valuable feedback.

References

Alonso, E.E., Gens, A., Josa, A., 1990. A constitutive model for partially saturated soils. Géotechnique 40 (3), 405–430. https://doi.org/10.1680/geot.1990.40.3.405.

ASTM, 2014a. ASTM D854–14: Standard Test Methods for Specific Gravity of Soil Solids by Water Pycnometer. West Conshohocken, P.A.

ASTM, 2014b. ASTM D4546–14: Standard Test Method for One-Dimensional Swell or Collapse of Soils. Technical report, West Conshohocken, P. A.

ASTM, 2017a. ASTM D6913 / D6913M-17: Standard Test Methods for Particle-Size Distribution (Gradation) of Soils Using Sieve Analysis. West Conshohocken, P.A.

ASTM, 2017b. ASTM D7928–17: Standard Test Method for Particle-Size Distribution (Gradation) of Fine-Grained Soils Using the Sedimentation (Hydrometer) Analysis. West Conshohocken, PA.

ASTM, 2017c. ASTM D4318-17e1: Standard Test Methods for Liquid Limit, Plastic Limit, and Plasticity Index of Soils. West Conshohocken, P. A.

ASTM, 2017d. ASTM D2487-17e1: Standard Practice for Classification of Soils for Engineering Purposes (Unified Soil Classification System). West Conshohocken, P. A.

Bishop, A.W., 1959. The Principle of Effective Stress. Teknick Ukeblad, 39, pp. 859–863.

Blight, G.E., 1984a. Power station foundations in deep expansive soil power station foundations in deep expansive soil. In: First International Conference on Case Histories in Geotechnical Engineering, Missouri, pp. 77–86.

Blight, G.E., 1984b. Uplift forces measured in piles in expansive clay. In: Fifth International Conference on Expansive Soils, Adelaide, South Australia, pp. 240–244.

Bosch, J.A., Ferrari, A., Laloui, L., 2021. Coupled hydro-mechanical analysis of compacted bentonite behaviour during hydration. Comput. Geotech. 140, 104447. https://doi.org/10.1016/j.compgeo.2021.104447.

Brackley, I.J.A., 1973. Swell pressure and free swell in a compacted clay. In: 3rd International Conference on Expansive Clays, vol. 1. Israel Institute of Technology, Haifa, Israel, pp. 169–176.

Brackley, I.J.A., Sanders, P.J., 1992. In situ measurement of total natural horizontal stresses in an expansive clay. Géotechnique 42 (3), 443–451.

BSI, 1990. BS 1377:1990: Methods of Test for Soils for Civil Engineering Purposes. BSI, London, UK.

Burland, J.B., 1990. On the compressibility and shear strength of natural clays (30th Rankine Lecture). Géotechnique 40 (3), 329–378.

Byrne, G., Chang, N., Raju, V., 2019. A Guide to Practical Geotechnical Engineering in Africa, Fifth Edition Edition. FRANKI A KELLER COMPANY.

Caicedo, B., Medina, C., Cacique, A., 2006. Validation of time scale factor of expansive soils in centrifuge modeling. International Conference on Physical Modelling in Geotechnics, 06, pp. 273–277.

Carey, T., Gavras, B., Kutter, B., Haigh, S.K., Madabushi, S.P.G., Okamura, M., Kim, D.S., Ueda, K., Hung, Y.G., Zhou, Y.G., Liu, K., Chen, Y.M., Zeghal, M., Abdoun, T., Escoffier, S., Manzari, M., 2014. A new shared miniature cone penetrometer forcentrifuge testing. In: Proceedings of the 9th International conference on Physical Modelling in Geotechnics.

Chandler, R.J., Apted, J.P., 1988. The effect of weathering on the strength of London Clay. Q. J. Eng. Geol. 21, 59–68.

Chen, T., Zhou, C., Wang, G., Liu, E., Dai, F., 2017. Centrifuge model test on unsaturated expansive soil slopes with cyclic wetting–drying and inundation at the slope toe. Int. J. Civ. Eng. **16** (6) https://doi.org/10.1007/s40999-017-0228-1.

Clayton, C.R.I., Matthews, M.C., Simons, N.E., 1995. Site Investigation. Oxford Wiley-Blackwell.

Day, P., 2020. Personal Communication.

Elsharief, A., 2012. Foundations on Expansive Soils, Sudan Experience. Graduate School Conference, on Basic Sciences and Engineering. University of Khartoum.

Fredlund, D.G., 2018. Role of the soil–water characteristic curve in unsaturated soil mechanics. In: Ng, C.W.W., Leung, A.K., Chiu, A., Zhou, C. (Eds.), The 7th International Conference on Unsaturated Soils, Hong Kong, pp. 3–26.

Fredlund, D.G., Morgenstern, N.R., 1977. Stress state variables for saturated and unsaturated soils. J. Geotech. Eng. Div. ASCE 103, 447–466.

Gaspar, T.A.V., 2020. Centrifuge Modelling of Piled Foundations in Swelling Clays. PhD Thesis,. University of Pretoria, Pretoria, South Africa.

Gaspar, T.A.V., Jacobsz, S.W., Heymann, G., Toll, D.G., Gens, A., Osman, A.S., 2022. The mechanical properties of a high plasticity expansive clay. Eng. Geol. 303 (March) https://doi.org/10.1016/j.enggeo.2022.106647, 106647.

Gu, X.W., Zhang, W.M., Xu, G.U., 2010. Earth pressure at rest of expansive soil against retaining wall. In: Springman, S., Laue, J., Seward, L. (Eds.), Proceedings of the 7th International Conference on Physical Modelling in Geotechnics (ICPMG 2010). Switzerland, Zurich, pp. 443–448.

Han, J., Yin, Z.Y., Dano, C., Hicher, P.Y., 2022. Undrained monotonic and cyclic behavior of a stiff fissured overconsolidated clay. Eng. Geol. 302 (March) https://doi.org/10.1016/j.enggeo.2022.106627, 106627.

Heymann, G., Clayton, C.R.I., 1999. Block sampling of soil: Some practical considerations. In: Wardle, G.R., Blight, G.E., Fourie, A. (Eds.), Geotechnics for Developing Africa, Durban, South Africa. Balkema/Rotterdam/Brookfield, pp. 331–339.

Jacobsz, S.W., Kearsley, E.P., Kock, J.H.L., 2014. The geotechnical centrifuge facility at the University of Pretoria. In: Gaudin, C., White, D. (Eds.), Physical modelling in Geotechnics: Proceedings 8th ICPMG. Perth, Australia. CRC Press, pp. 169–174.

Jiang, G., Chen, W., Liu, X., Yuan, S., Wu, L., Zhang, C., 2018. Field study on swelling-shrinkage response of an expansive soil foundation under high-speed railway embankment loads. Soils Found. 58 (6), 1538–1552. https://doi.org/10.1016/j.sandf.2018.09.008.

Laporte, S., Siemens, G.A., Beddoe, R.A., 2018. Physical modelling of roads in expansive clay subjected to wetting–drying cycles. In: McNamara, A., Divall, S., Goodey, R., Taylor, N., Stallebrass, S., Panchal, J. (Eds.), Proceedings of the 9th International Conference on Physical Modelling in Geotechnics (ICPMG 2018), London, United Kingdom, pp. 175–178.

Lu, N., Likos, W., 2004. Unsaturated Soil Mechanics. John Wiley & Sons, Inc., Hoboken, New Jersey.

Manca, D., Ferrari, A., Laloui, L., 2016. Fabric evolution and the related swelling behaviour of a sand/bentonite mixture upon hydro-chemo-mechanical loadings. Géotechnique 66 (1), 41–57. https://doi.org/10.1680/jgeot.15.P.073.

Meintjes, H.A.C., 1991. A case history on heaving clay: Colinda primary School. In: Blight, G.E., Fourie, A.B., Luker, I., Mouton, D.J., Scheurenberg, R.J. (Eds.), Geotechnics in the African Environment, Maseru, Lesotho. Balkema, Rotterdam, pp. 99–104.

Meintjes, H.A.C., Pellissier, J.P., 1994. An experimental pile in deep residual expansive clay. In: Proceedings of the 13th International Conference on Soil Mechanics and Foundations Engineering, New Dehli, India, pp. 487–492.

Meter Group, 2017a. 5TM User's Manual. Meter Group.

Meter Group, 2017b. Teros 21. User Manual. Meter Group.

Monroy, R., Zdravkovic, L., Ridley, A.M., 2015. Mechanical behaviour of unsaturated expansive clay under K0 conditions. Eng. Geol. 197, 112–131. https://doi.org/10.1016/j.enggeo.2015.08.006.

Moses, A.M., 2008. Mineralogy, Chemistry and Pedological Investigations of the Maandaagshoek 254 kt's Palygorskite deposit: Implication on the Genesis and Industrial Application. University of Pretoria, Technical report.

Ng, C.W.W., Zhan, L.T., Bao, C.G., Fredlund, D.G., Gong, B.W., 2003. Performance of an unsaturated expansive soil slope subjected to artificial rainfall infiltration. Géotechnique 53 (2), 143–157. https://doi.org/10.1680/geot.53.2.143.37272.

Novak, V., Simunek, J., Genuchten, M.T., 2000. Infiltration of water into soil with cracks. J. Irrig. Drain. Eng. 126 (1), 41–47. https://doi.org/10.1061/(ASCE)0733-9437(2000)126:1 (41).

Plaisted, M.D., Zornberg, J.G., 2010. Testing of an expansive clay in a centrifuge permeameter. In: Springman, S., Laue, J., Seward, L. (Eds.), Proceedings of the 7th International Conference on Physical Modelling in Geotechnics (ICPMG 2010), Zurich, Switzerland, pp. 1477–1481.

Rao, S.M., 2006. Identification and Classification of Expansive Soils. Expansive Soils-Recent Advances in Characterization and Treatment. Taylor & Francis, London, pp. 15–24.

Romero, E., Simms, P.H., 2008. Microstructure investigation in unsaturated soils: a review with special attention to contribution of mercury intrusion porosimetry and environmental scanning electron microscopy. Geotech. Geol. Eng. 26, 705–727. https://doi.org/10.1007/s10706-008-9204-5.

Schreiner, H.D., 1988. Volume Change of Compacted Highly Plastic African Clays. PhD thesis,. Imperial College London.

Schreiner, H.D., Burland, J.B., 1991. A comparison of three swell test procedures. In: Blight, G.E., Fourie, A.B., Luker, I., Mouton, D.J., Scheurenberg, R.J. (Eds.), Geotechnics in the African Environment, Maseru, Lesotho, vol. 1. Balkema, Rotterdam, pp. 259–266.

Sridharan, A., Rao, A.S., Sivapullaiah, P.V., 1986. Swelling pressure of clays. Geotech. Test. J. 9 (1), 24–33.

Thorne, C.P., 1984. Strength assessment and stability analyses for fissured clays. Géotechnique 34 (3), 305–322.

Toll, D.G., Rahim, M.S., Karthikeyan, M., Tsaparas, I., 2018. Soil - atmosphere interactions for analysing slopes in tropical soils in Singapore. Environ. Geotechnics 6 (6), 361–372.

Topp, G.C., 1980. Electromagnetic determination of soil water content: measurement in coaxial transmission lines. Water Resour. Res. 16 (3), 574–582.

Tripathy, S., Al-Khyat, S., Cleall, P.J., Baille, W., Schanz, T., 2016. Soil suction measurement of unsaturated soils with a sensor using fixed-matrix porous ceramic discs. Indian Geotech. J. 46 (3), 252–260.

Van der Merwe, D., 1964. The prediction of heave from the plasticity index and percentage clay fraction of soils. In: *The Civil* Engineer, pp. 103–107.

Van Genuchten, M.T., Schaap, M.G., Mohanty, B.P., Simunek, J., Leij, F.J., 1999. Modeling flow and transport processes at the local scale. In: Feyen, J., Wiyo, K. (Eds.), Modeling of Transport Process in Soils at Various Scales. Wageningen Pers, Wageningen, the Netherlands, pp. 23–45.

Vanapalli, S.K., Fredlund, D.G., Pufahl, D.E., 1999. The influence of soil structure and stress history on the soil-water characteristics of a compacted till. Géotechnique 49 (2), 143–159.

Williams, A.A.B., 1991. The extraordinary effect of chemical heaving and its effect on buildings and roads. In: Blight, G.E., Fourie, A.B., Luker, I., Mouton, D.J., Scheurenberg, R.J. (Eds.), Geotechnics in the African Environment, Maseru, Lesotho. Balkema, Rotterdam, pp. 91–98.